Title

The Reactive—Diffusive Length of OH and Ozone in Model Organic Aerosols

Journal

The Journal of Physical Chemistry A, 120(34)

ISSN

1089-5639

Authors

Lee, Lance

Wilson, Kevin

Publication Date

2016-09-01

DOI

10.1021/acs.jpca.6b05285

Peer reviewed

The Reactive-Diffusive Length of OH and Ozone in Model Organic Aerosols

*Lance Lee and Kevin Wilson**

[1]Chemical Sciences Division, Lawrence Berkeley National Laboratory, Berkeley, California 94720, USA

*Correspondence to: (510) 495-2474, krwilson@lbl.gov.

Abstract

A key step in the heterogeneous oxidation of atmospheric aerosols is the reaction of ozone (O_3) and hydroxyl radicals (OH) at the gas-particle interface. The formation of reaction products and free radical intermediates and their spatial distribution inside the particle is a sensitive function of the length over which these oxidants diffuse prior to reaction. The reactive-diffusive length of OH and ozone at organic aerosol interfaces is determined by observing the change in the effective uptake coefficient for size-selected model aerosols comprised of a reactive core and a thin nanometer-sized (0-12 nm) organic shell . The core and shell materials are selected so that they are immiscible and adopt an assumed core-shell configuration. The results indicate a reactive-diffusive length of 1.4 nm for hydroxyl (OH) radicals in squalane and 1.0 nm for ozone in squalene. Measurements for a purely diffusive system allows for an estimate for diffusion constant (1.6×10^{-6} cm^2/s) of ozone in squalane to be determined. The reactive-diffusive length offers a simple first order estimate of how shielding of aerosols by immiscible layers can alter estimates of oxidative lifetimes of aerosols in the atmosphere.

I. Introduction

Aerosols affect the radiative budget of the Earth's atmosphere both directly through light absorption and scattering, and indirectly through modification of cloud formation and cloud lifetime [1]. An important source of tropospheric aerosols is related to anthropogenic activities, especially from combustion related processes (motor oil, unburnt fuel, etc.) [2-5]. These aerosols typically contain a substantial amount of organic material that can be transformed in the atmosphere by chemical reactions. Heterogeneous oxidation of aerosols occurs when an oxidant such as O_3 or OH collides and reacts with molecules at the particle surface [6]. The chemical transformation rate and product formation pathways have been shown to be a complex function of both the diffusion rate of organics to the aerosol particle surface as well as the diffusion of gas phase oxidants into the subsurface and interior of the particle. Thus, a key parameter in any heterogeneous reaction is the reactive-diffusive length, which governs where the reaction occurs (surface vs. subsurface vs. bulk) and the overall spatial distribution of reaction products and intermediates in the aerosol particle.

For organics that are sufficiently fluid (diffusion timescales shorter than the chemical lifetime in the reaction region), there is no transport limitations for bulk phase material to migrate to the gas-particle interface between reactive gas phase collisions. In this case, no radial gradients in particle composition are expected. However, when the mobility of the organic material approaches that of glass, semi-solid or solid, uneven oxidation of the particle occurs leading to chemical gradients and significant changes in the heterogeneous reaction rate (i.e. uptake coefficient)[7-8]. Under these conditions, the diffusive mixing length scale of organic material can be reduced to that of small reactive oxidants (e.g. O_3 and OH) so that the movement of both must be considered for an accurate description of the heterogeneous reaction. Furthermore, the oxidative

age of the organic molecules within aerosols becomes a function of its location in the particle rather than being simply controlled by the oxidant-surface collision rate. As a consequence, the volume-averaged composition of an aerosol particle may not be representative of its surface with possible larger impacts on water uptake and toxicity [9].

To determine the chemical lifetime of organic particles during heterogeneous oxidation, reactive uptake coefficients have been measured between numerous aerosol particle proxies and gas phase oxidants [10-14]. A reactive uptake coefficient (γ) is simply the fraction of gas collisions with the aerosol particle surface that yield a reaction. For example, many laboratory studies measured the reaction of ozone (O_3), a relatively long-lived oxidant, on various organic aerosol particle proxies representing liquid [15], solid [16-17] or mixed [7-8, 18] states to investigate how the matrix diffusivity impacts effective uptake coefficients. These measurements offered some insight into the diffusion length of O_3 in the condensed phase (the reactive-diffusive length of O_3) in various organic matrices since the reactive aerosol particle volume controls the overall consumption rate of ozone. However, clear interpretations are sometimes difficult since a change in uptake coefficient may include coupled effects when varying the diffusivity of the matrix and/or surface to volume ratio of the aerosol particle [15]. As most measurements observe the reactive decay of a particle phase species to determine γ, rather than the consumption of the gas phase oxidants directly, additional uncertainties arise as secondary reactions could also occur as the organic phase is changed.

An alternative way to quantify the reactive-diffusive lengths of small oxidants is to measure their transmission efficiency through a barrier. There has been some earlier experiments investigating the heterogeneous reactivity of organic molecules at "buried interfaces" such as those reported by Zhou et. al. [19-20] and by Kolesar et. al. [21]. In Zhou et. al. benzopyrene was allowed to

diffuse through a non-reactive layer to reach the gas-particle interface where it undergoes reaction with gas phase ozone. Both liquid and solid layers were prepared and a reduction in reactivity was observed most notably when benzopyrene was buried under a solid layer. Kolesar et al. coated liquid squalane particles with secondary organic aerosols (SOA) produced from α-pinene ozonlysis and then observed the decay of squalane signal as a function of OH exposure. It was found that squalane reacted more quickly with the SOA coating than without it. It is currently unclear how the coating enhanced squalene reactivity but could originate from secondary free radical reactions produced in the SOA coating. Here we use another technique that allows for direct measurements of the reactive-diffusive length of ozone and OH radical in model aerosols using size-selected core-shell particles in a flow tube reactor.

II. Experimental Approach and Modeling Methods

To quantify the reactive-diffusive length of OH or ozone, our experimental approach is based upon a barrier-crossing configuration. This is done by first introducing oxidants at one side of a barrier and then allowing them to diffuse and/or react while monitoring the amount of oxidant that passes through to the other side. The transmission of oxidants as a function of the barrier width should then provide direct information on the reactive-diffusive properties of the barrier material itself. This geometry is achieved by making core-shell aerosols where the shell consists of material for which the diffusive-reactive characteristics are known or can be determined. The core material, buried beneath the shell barrier, is used as a detector for the quantity of oxidants that traverse the barrier by monitoring the chemical reaction of the core material with the oxidant.

Phase separation is key to maintaining a well-defined barrier layer so the core should be chemically distinct and immicible with the shell material. We are interested in the reactive-diffusive behavior of O_3 and OH in organic aerosols and use squalane ($C_{30}H_{62}$, branched alkane)

and squalene ($C_{30}H_{50}$, a branched alkene with 6 double bonds), as simple organic aerosol proxies. To satify the above requirements, *trans*-aconitic acid ($C_6H_6O_6$, Fig. 1) is used as the core material for ozone experiments and D-mannitol ($C_6H_{14}O_6$, Fig. 1) for OH experiments, both purchased directly from Sigma Aldrich. In the following sections we describe the experimental approach (Section IIa-d) and modeling methods (Section IIe). A general schematic of the experimental setup is shown in Fig. 2.

a. Aerosol particle generation

Size-selected core-shell particles of specific composition are generated in a series of steps, as shown in Fig. 2. An aqueous solution of the core material is first atomized and dried over silica gel to a relative humidity (RH) below 15%. This yields a stream of polydisperse solid aerosols, which is then size-selected using a scanning mobility particle sizer (SMPS, TSI Inc.). The typical core diameter used in these experiments is between 60 and 104 nm. The resulting monodisperse core stream is then passed through an annular charcoal denuder to eliminate any unwanted volatile contaminants. The core is then pass through a pyrex tube located in a furnace [22] containing the organic compound for the shell coating (e.g. squalene and squalene). The coating forms on the core via heterogeneous nucleation upon exiting the heated section of the oven. The thickness of the coating is controlled by varying the temperature of the oven, as shown in Fig. 3. The width of the coating thickness increases as a function of average coating thickness. In general, the narrowest distribution of coating thickness is obtained when the average coating thickness is around 1 to 2 nm. Fig. 4 shows the particle size distribution measured at the end of the flow tube for aerosols with and without a coating of squalene on a 63 nm *trans*-aconitic acid core. The satellite peaks in the size distribution result from doubly charged particles being re-normalized by the bipolar charger of the measuring SMPS. It is worth noting that as a consequence of heterogeneous

nucleation, the particles have essentially the same coating thickness regardless of the core size. For example, for core diameters centered at 62.7 nm and 90.5 nm a ~4 nm shell thickness is observed after passing through the oven. No significant evaporation of core material or homogeneous nucleation of the shell material was observed. The final size of the core-shell particle was measured using a second SMPS located after the end of the flow tube reactor in the absence of oxidants. Our experimental observations support the assumption of core-shell morphology, as will be shown in the results section.

b. Flow tube reactor

Details of the flow tube setup have been described previously[23]. All oxidation experiments were carried out at 20°C under ambient pressure and 45% RH. The aerosol stream was mixed with a dilution flow containing N_2, O_2 and a gas phase tracer (i.e. a kinetic reference) with a well-known rate coefficient for the reaction with either O_3 or OH. The thermostated double-walled quartz flow tube reactor has an internal diameter of 36 mm and a length of 244 cm. While operating under laminar flow regime with a total gas throughput of ~1100 standard cubic centimeter per minute (sccm), the centerline velocity yields a residence time of ~70 seconds. The aerosols and gas phase reference compound were sampled through the same port near the center of the flow tube. For heterogeneous reactions with ozone, the flow tube enclosure was kept dark and O_3 was generated externally using a corona discharge and/or a mercury pen-ray lamp. O_3 is introduced separately near the head of the flow tube. Propane was added to the dilution flow as an OH scrubber during O_3 experiments. For OH oxidation experiments, OH was generated *in situ* by the photolysis of O_3 in the presence of water vapor by illuminating the flow tube enclosure with germicidal lamps at 254 nm. Gas chromatography was used to detect the decay of reference compound to quantify the

oxidant concentrations. Changes in the size of oxidized aerosols are monitored with a second SMPS at the end of the flow tube.

c. Mass spectrometry

A Q Exactive orbitrap mass spectrometer (Thermo Fisher), equipped with a DART (Direct Analysis in Real Time, DART SVP, Ion Sense) evaporation/ionization source, is used for analyzing aerosol composition. In DART, metastable helium atoms are generated via an electrical discharge and carried to the interaction region in a flow of heated helium gas. When this helium gas is mixed with the aerosol flow near the spectrometer inlet, the aerosol particles are completely vaporized and then ionized. The helium flow rate in the DART source is ~3 liter per minute and an internal temperature of 500°C. To reject gas phase contribution to the mass signal, an activated charcoal denuder with square channels (MAST Carbon Inc.) is positioned between the flow tube and the mass spectrometer. The complete evaporation of the particle was confirmed separately by sampling the combined flow using a SMPS. Exact masses of negative ions were monitored. The reactive decay of the parent ion of the core was used for the subsequent analysis.

d. Uptake coefficients

The loss of condensed phase organic is measured instead of the loss of original gas phase oxidant. Therefore, an effective uptake coefficient (γ) is defined as the amount of particle-bound organics lost divided by the total number of collisions by gas phase oxidant with the particle surface. For the case of a strictly one-to-one consumption of the oxidant and particle-bound organic in the absence of secondary reactions the two approaches for determining γ are equivalent. The total number of surface collisions by the gas phase oxidant is computed from the decay of reference compounds, while the consumption of particle phase material is monitored using mass spectrometry. The value of γ is then calculated using Eq. 1,

$$\Delta \ln(C) = \frac{\gamma \langle v \rangle A}{4 C_0 k_{ref}} \Delta \ln\left(n_{ref}\right) \quad (1)$$

where C_0 and C are the initial and current concentration of particle phase organic, respectively. n_{ref} is the current gas phase concentration of reference compound, k_{ref} the rate constant of the reference compound with the oxidant, <v> the mean speed of the oxidant, and A the surface area of the particle. It is assumed that all particle phase organics have the same probability to react and the overall condensed phase reactivity remains constant. This requirement is satisfied if the measurements are conducted over the early stages of particle oxidation. We therefore limit the extent of oxidation for each experiment to within 30% consumption of initial core material, a condition which maintains the the relationship predicted by Eq. 1. Gas phase diffusion limitations of the oxidants are negligible for the particle sizes used here (~100 nm) and are thus neglected.

e. Barrier coefficient

The presence of a barrier controls the amout of oxidant that reaches the core material. Ideally the core material should be infinitely reactive toward the target oxidants to achieve an uptake coefficient of unity (a perfect sink). Since in reality this is not possible, we account for this by simply normalizing observed uptake coefficients for the core-shell particles (γ) to the bare core value (γ_0), measured without any coating material. This effectively cancels out the contribution of the core due to the possibility of secondary reactions as well as its finite reactivity. For simplicity, we refer to this ratio (γ/γ_0) as the "barrier coefficient" in the subsequent text.

The relationship between the value of the barrier coefficient and shell thickness is controlled both by the diffusion constant (D) of the oxidant (i.e. O_3 or OH) in the shell and any reactions between molecules (i.e. squalene or squalene) in the shell and the oxidants. The barrier coefficient vs. shell thickness is computed by solving the Fickian diffusion equation with an

additional chemical consumption term (for the case of a reactive shell) in a spherically symmetric core-shell volume. The mathematical details are included in the Appendix.

Briefly, the observed dependence of the barrier coefficient on shell thickness can be fit by the function (γ/γ_0) derived from the analytical solution of the oxidant concentration ($\rho(r)$) as a function of radius (r) using a single parameter. For O_3 experiments using a non-reactive shell this parameter is simply the diffusion coefficient of O_3 in squalane. For O_3 experiments using a reactive squalene shell as well as the OH experiments this single parameter is the reactive diffusive length L expressed in terms of diffustion constant D and chemical lifetime τ in Eq. 2.

$$L = \sqrt{D \cdot \tau} \tag{2}$$

The chemical lifetime can be calculated as the pseudo first order rate constant of radicals in excess of organics. We note that it is possible to obtain properties of the core by fitting the bare core γ value measured with Eq. 3 and recognizing r_1 as the radius of the core.

$$\gamma = \frac{\frac{4\pi}{\tau}\int_0^{r1}\rho(r)r^2dr}{\frac{\langle\nu\rangle}{4}A\cdot n} \tag{3}$$

However, our current measurements are not sufficiently constrainted and the solutions are not unique.

Fig. 4 illustrates these two distinct cases with example functions of $\rho(r)$ with r_1 and r_2 corresponding to the radial location of the core-shell and particle-air interfaces, respectively. The rate of decay of $\rho(r)$ in the shell affects the barrier coefficient. Since γ can be expressed as a function of $\rho(r)$ as shown in Eq. 3, the barrier coefficient effectively probes the ratio of total oxidant concentration in the core region after transmission through the shell normalized to the bare core value. It is interesting to note here that although for a non-reactive shell the oxidants are not

consumed during transmission, there remains a decrease in the consumption rate at the core simply due to the attenuation in oxidant concentration ρ reaching the r_1 interface compared with ρ at r_2.

A number of assumptions are made in solving ρ(r) analytically. First, it is assumed that the Henry's law constants of the oxidants are similar in both the shell and core material. This assumption appears reasonable since there is not an abrupt change in γ for coated vs. uncoated experiments, which indicates that the Henry's law constant of either O_3 or OH in squalane or squalene is not substantially different than that in *trans*-aconitic acid or D-mannitol. Second it is assumed that the chemical lifetime of the oxidant remains independent of the age of the shell or core organics, which is valid for small extents of reaction. This assumption appears reasonable since, we did not observe any significant deviation from the linear relationship predicted in Eq. 1, with or without coatings for the O_3 experiments. For OH experiments the same argument cannot be strictly applied since the coating thickness changes during oxidation, due to the production of reaction products that evaporate from the particle (e.g. Smith et al. [22]). However, the analytical solution can still account for the data satisfactorily with a constant chemical lifetime and it appears the τ does not deviate from the original value by more than a factor of 2 from sensitivity analysis of the fit. Finally, it is assumed that no discontinuity in oxidant concentration exists at the shell-core interface (i.e. r_1). If a discontinuity were to exist, corrections to γ can be made if we define a factor (β) to represent the ratio of $\rho_2(r_1)/\rho_1(r_1)$ where $\rho_1(r_1)$ and $\rho_2(r_1)$ describes interfacial oxidant concentrations in the core and shell regions, respectively. For both reactive or non-reactive shells under our experimental condition γ scales approximately with 1/β. It was not necessary to use a value of β significantly different from 1 in this work. For simplicity, we use β = 1 for all subsequent analysis. The parameters for constructing $\rho_1(r)$ in the core region are adjusted to satisfy the bare core γ values. The value of (γ/γ_0) is generally insensitive to these core parameters.

III. Results and Discussion

The following sections are organized as follows: Section IIIa and IIIb report O_3 experiments on non-reactive (squalane) and reactive (squalene) shells, respectively. Experimental data are presented first, followed by results and discussions. In section IIIc OH experiments on reactive (squalane) shells are presented followed by a discussion. In section IIId additional free radical chemistry produced by OH oxidation is examined, potentially altering the transmission through the reactive shell.

a. Ozone transmission through unreactive shell

For the purely diffusive ozone system squalane was used as the shell material and *trans*-aconitic acid as the core. γ_0, measured in the absence of coating, is $(5.1\pm0.1)\times10^{-7}$ where the uncertainty represents the 95% confidence interval of the slope derived from the data shown in Fig. 6. This linear relationship is expected from Eq. 1, and inclusive of any possible secondary reactions. This value for γ_0 is in agreement with literature values of structurally similar compounds with a single C=C bond, such as maleic acid ($1.7 - 0.5 \times10^{-7}$) and fumaric acid ($1.4 - 0.6\times10^{-7}$) measured under dry conditions [16]. As the deliquescence point of pure maleic acid is known (~90% relative humidity) [24], we assume *trans*-aconitic acid core to be also in the dry state at a relative humidity of 45% in the flow tube.

A series of experiments with varying coating thicknesses of squalane on *trans*-aconitic acid core are summarized in Table 1. The typical particle number concentration during experiments is $\sim1\times10^4$ cm^{-3}. Two gas phase reference compounds were used to span the wide range of O_3 exposures, which are necessary to achieve similar levels of core material consumption from the bare core to > 8 nm coating thickness. Typically 3,3-dimethyl-1-butene (dmB) was used for thin coatings with O_3 exposure up to 5×10^{17} $cm^{-3}\cdot s$ and allene for coating thickness in excess of 4 nm.

Ozone reaction rate constants for dmB and allene are 3.9×10^{-18} $cm^3\cdot s^{-1}$ [25] and 1.53×10^{-19} $cm^3\cdot s^{-1}$ [26], respectively. The barrier coefficient is plotted as a function of squalene coating thickness and is shown in Fig. 7.

For a purely diffusive shell, the decrease in apparent uptake coefficient shown in Fig. 7 is directly related to the concentration gradient that is required to establish an inward ozone flux that matches the total ozone consumption rate by the reactive core. As illustrated by case 2 in Fig. 5, the concentration profile $\rho(r)$ of O_3 in the shell follows a 1/r dependence in the absence of local sink. The relative decrease in uptake coefficient is directly proportional to the ozone consumption rate by the core, reflected by the sustained O_3 concentration at the r_1 interface $\rho(r_1)$. Eq. 4 represents $\rho(r_1)$ as a function of the total O_3 consumption rate X, the interfacial equilibrium ozone concentration $\rho_0(r_2)$ and the effective flux resistance due to the diffusion term (R_D) and surface collision term (R_c).

$$\rho(r_1) = \frac{\rho_{0(r_2)}}{1+X\cdot R_D+X\cdot R_C} \tag{4}$$

Note that when the core is unreactive (X=0), the O_3 concentrations across the shell region become the same and equal to the equilibrium value $\rho_0(r_2)$. The final equation for $\rho(r_1)$ can be solved by replacing X with an explicit function of $\rho(r_1)$ and then by rearrangement of terms (see Appendix). We fit the barrier coefficient obtained experimentally with an analytical solution of γ/γ_0 by adjusting only the diffusion coefficient of ozone in squalane. The value that best replicates the data is $D_{O3} = 1.6\times10^{-6}$ cm^2/s at 20°C.

The diffusion coefficient of ozone in squalane can be compared to an estimation method derived from tracer diffusion experiments in organic compounds reported by Evans et al. [27]. Such an estimate requires both the Van der Waals radius of the solute (O_3) and the viscosity of the

solvent (squalane). Communes et al. [28] reported a value of 36.1 mPa·s at 20°C for the viscosity of squalene. The collisional radius of O_3 (1.8 Å) is obtained by taking the cubic root of molecular volume of liquid ozone at 77K using the liquid density data [29] then dividing by 2. Using these values we obtained an estimate of $D_{O3} = 2.7\times10^{-6}$ cm^3/s, which is 66% larger than our experimental result. It is likely that the hard-sphere estimation of the O_3 collisional radius is the cause of this overestimation in diffusivity because the quoted collisional radius of N_2 in Evans et al. is 1.93 Å, a value larger than what we used for O_3. In the absence of more direct data, our experimental value appears quite reasonable for ozone diffusivity in large organic solvents.

b. Ozone Transmission through Reactive shell

To examine the transmission of O_3 through a reactive shell, squalene is used as the coating material. Squalene has 6 double bonds, which readily react with ozone. The core composition is altered because squalene appears to have a low coating affinity on pure *trans*-aconitic acid surfaces. By doping the core with approximately 30% of D-mannitol, a chemically inert component towards ozone oxidation, consistent and reproducible coatings were acheived. The addition of mannitol enhances γ_0 of the bare core to approximately twice the value as previously measured (i.e. pure *trans*-aconitic acid, see Table 2). This is simply due to dilution of the core material. In a diluted core of the same size, there are now fewer *trans*-aconitic acid molecules present. Since the additive (D-mannitol) does not react with O_3, the relative decay of *trans*-aconitic acid will appear faster after the same number of O_3 reactions when plotted as the natural log. Again the core effect is compensated for by taking the ratio of (γ/γ_0) as discussed above. The barrier coefficient as a function of squalene coating thickness is plotted in Fig. 7. We point out there that the observed decrease in the barrier coefficient is consistent with a core-shell aerosol morphology. If mixing were to occur during the generation process (e.g. in the oven), the shell material would

be diluted substantially by the core material and a much weaker shielding effect would be observed. For example, at a 2 nm coating thickness squalene would account for a mole fraction of ~17% when mixed with the core material. This can only amount to a ~50% reduction in the consumption rate of *trans*-aconitic acid, instead of the observed 90%. A similar argument applies for the OH system.

For this system O_3 undergoes reactive loss, while diffusing through the shell region. This reaction further reduces the concentration of O_3 reaching the core, as illustrated in Fig. 5, case 1. A more rapid decrease of the barrier coefficient as a function of coating thickness is expected and confirmed by our measurements. The barrier coefficient follows a functional form that can be derived from $\rho(r)$ as constructed from connecting general solutions in both core and shell regions, as detailed in the Appendix. The analytical solution of γ/γ_0 is fit to the observation by adjusting L, the reactive-diffusive length. The best description of the experimental measurement is achieved when L = 1.03 nm.

L determines the decay constant as shown in Fig. 7. It is reasonable to assume that D_{O3} in squalene is the same as that in squalene; [30] thus the same diffusion coefficient ($D_{O3} = 1.6\times10^{-6}$ $cm^2\cdot s^{-1}$) is used to compute the reactivity of ozone in squalene. The chemical lifetime of ozone in a pure squalene matrix is $\tau = 6.6\times10^{-9}$ s, or if converted to a typical condensed phase second order reaction rate constant by accounting for the molarity of pure squalene (1.9 M), 7.3×10^7 $M^{-1}s^{-1}$. This lifetime is considerably shorter than those extrapolated from gas phase O_3 reactions of 2-methyl-2-butene ($\tau = 4.3\times10^{-7}$ s) and 2,3-dimethyl-2-butene ($\tau = 1.8\times10^{-7}$ s) as well as much faster than the available literature on solution phase reaction rate constants for ozone reactions with ~0.2 M squalene solution in CCl_4, (7.5×10^5 $M^{-1}s^{-1}$) [31-32]. A chemically similar system of poly-isoprene dissolved in CCl_4 reacts with ozone at a similar rate constant of 4.4×10^5 $M^{-1}s^{-1}$ [32].

The measurements reported here are at least an order of magnitude higher in organic concentration than the most concentrated cases reported in literature, and as such additional O_3 reactions may contribute to the much shorter lifetime observed here. The reaction of Criegee intermediates with O_3 does not appear to constitute a significant sink for O_3 when compared to its native squalene reactivity (different by a factor of 10^{-3}), according to the work by Epstein and Donahue[33] on the Criegee decomposition pathways and Vereecken et al.[34] who calculated the rate constant. Even if we assume that the O_3 lifetime in squalene is 7×10^{-7} s (from ref. 31), the corresponding diffusion constant D_{O3} would need to be around 2.5×10^{-8} $cm^2\cdot s^{-1}$ to yield L = 1.03 nm and match the data shown in Fig. 7. This value appears to be unreasonably small since the the self-diffusion constant of squalane has been measured to be 3×10^{-7} $cm^2\cdot s^{-1}$ [30]. To our knowledge, direct experimental measurements on the chemical lifetime of ozone in a pure unsaturated organic matrix is not available for comparison and additional investigations are necessary to identify the origin of the accelerated reactivity. In spite of the difference in inferred O_3 lifetime, we demonstrate that the location of ozone reaction is indeed near the surface of the particle. This is consistent with results obtained from uptake coefficient measurements on size selected particles reported by Hearn et al. [15].

Recently, Zhou et al. [19-20] performed a number of barrier diffusion experiments on the heterogeneous reactivity of benzopyrene and ozone. Although the strategy for decoupling diffusion from reactivity is similar, the interpretations are quite different. Specifically, Zhou et al. measured the consumption rate of benzopyrene as a dopant in a diffusive shell made from high molecular weight components comprised of bis(2-ethylhexyl)sebacate, phenyl-siloxane oil, eicosane and α-pinene SOA. Benzopyrene can diffuse through the ozone-inert organic shell to reach the surface where it is oxidized by O_3. In the simulation of the data, it was assumed that

direct reaction between ozone and benzopyrene in the bulk is slow and that the dominant reactions proceed through reactive oxygen intermediates (ROI) at the surface. However, if a similar value for the bulk ozone reaction rate (5×10^{-18} $cm^3 \cdot s^{-1}$) as reported by Zhou et al. [20] was used in our system, it would yield a reactive-diffusive length of ~100 nm. This value is too large to cause significant depletion of O_3 for a coating thickness of ~2 nm, unless we were observing the diffusion behavior of a ROI-analog that could cause efficient consumption of aconitic acid. It remains uncertain if ROI-type reactions can be produced in aliphatic alkene reactions with ozone, as the formation of pre-reactive complex has only been calculated for larger polycyclic aromatic hydrocarbons [35]. Currently, we cannot rule out this possibility and further study on reaction products in the thin shell layer may provide the necessary clue.

c. OH Transmission through a reactive shell

For OH experiments a reactive squalane shell is applied to a ~88 nm diameter mannitol core. The γ_0 value of bare mannitol core was measured to be 0.53±0.04 and quantified using the gas phase tracer acetone. The rate constant for acetone + OH reaction is 1.89×10^{-13} $cm^3 \cdot s^{-1}$ [36]. This γ_0 value is similar to erythritol (0.77), a smaller molecular weight analog, measured by Kessler [37] under dry conditions. We expect the mannitol core to be also free of water since the deliquescence point is between 75% RH [38] and >90% [39], which is much higher than our experimental conditions (45% RH).

For coated experiments, uptake coefficient measurements were repeated at different initial squalene coating thicknesses. A notable shrinkage of the squalane shell during OH oxidation was observed and the particle coating thickness tended to decrease over the course of the reaction due to the production of volatile reaction products. This results in a curvature when plotting OH experimental data and a linear fit is no longer appropriate. Instead, γ is computed using 2

consecutive OH exposure measurements (Eq. 1) using concurrent measurements of particle size to obtain the appropriate particle surface area. Note that this method yields the same answer for experiments in which the coating thickness remains a constant during oxidation, such as O_3 experiments described above. Experiments are listed in Table 3. Fig. 8 shows the barrier coefficient as a function of squalane coating thickness. The experimental uncertainties are single point estimates from ion signal variation and the GC measurements.

Determination of reactive-diffusive length of OH in squalane follows the same procedure as described above for the ozone experiment. The piece-wise constructed solution was used to calculate the expected barrier coefficient of the OH radical through the squalane shell. The only adjustable parameter in the model is the reactive-diffusive length L. A value of L = 1.4 nm best describes the initial decay of the data. However, this fit (shown as a gold line in Fig. 8) does not satisfactorily capture the measurements beyond a coating thickness of 4 nm, where a much slower decay suggests an additional mechanism with a larger effective L. The possibilities include effects due to organic radicals that arise from the OH reaction with squalane, and a change in shell morphology. Although prior experiment with pure squalane do indicate any significant change in oxidation kinetics[22], the presence of mannitol core may have unexpected effects that cannot be constrained by our dataset. In the next section, we focus the evaluation on possible contributions of alkyl (R), alkyl peroxy (RO_2) and alkoxy radicals (RO) produced by the intial OH reaction in the squalene (RH) layer.

Using Eq. 2 the chemical lifetime or diffusion coefficient of the OH radical in squalane matrix can be computed if one of the variables is known. D_{OH} in squalane is expected to be larger than D_{O3} solely from the differences in collisional radius. From Easteal et al.,[40] who reported water diffusion in organic solvents, we extrapolate values obtained for hydrophobic solvents using the

viscosity of squalane at 36.1 mPa·s to obtain $D_{H2O} = 3.14\times10^{-6}$ $cm^2\cdot s^{-1}$ at 298K. This value appears reasonable relative to D_{O3} determined previously for ozone. For comparison, an estimate for methane [27] yields $D = 7.5\times10^{-6}$ $cm^2\cdot s^{-1}$ at 293K. For simplicity, we take an middle value of $D_{OH} = 4.8\times10^{-6}$ $cm^2\cdot s^{-1}$ in order to compute the OH chemical lifetime, which is determined to be $\tau = 4.1\times10^{-9}$ s, or in condensed phase rate units, 1.3×10^{8} $M^{-1}s^{-1}$. It is interesting to note that the lifetime of OH is only about 40% smaller than the lifetime of ozone in squalene.

Literature data on condensed phase OH reaction rate constant of octane in an aqueous solution reported by Rudakov [41] is 9.1×10^{9} $M^{-1}s^{-1}$, a value much larger than our estimate for squalane. There are significant differences between these experiments in which the octane concentration is small and the solvent is polar (water). Another comparison can be made using a more recent experiment on the OH oxidation of long chain water-soluble polymers (poly N-vinylpyrrolidone) measured over a wide range of concentrations. Bartoszek et al. [42] produced OH radicals by flash photolysis in an aqueous solution containing various concentrations of the polymers to study the effect of OH radical diffusion on the overall reaction rate towards the polymer. Assuming that OH is equally reactive towards hydrogen atoms located on the polymer and squalane, the chemical lifetime of OH in a solution of the highest polymer concentration (~1M, 76 kDa average molecular weight) is 8×10^{-10} s, a value within the same order of magnitude as our estimate for squalane. This agreement is perhaps reasonable considering that at high polymer concentrations, OH has a large probability of being produced in close proximity to the polymer and is less influenced by water, similar to the limiting case of a pure organic.

It may appear surprising that for the two systems (O_3 and OH) of vastly different heterogeneous reactivity (γ for OH reactive uptake on squalane is a ~1000 larger than the uptake coefficient for O_3 on squalene), the reactive-diffusive lengths are within the same order of

magnitude. This can be rationalized from gas-particle partitioning, a factor controlled by the Henry's law constant. For a single component system, L determines the steady state shape of ρ(r), but not the absolute value of the oxidant concentration. Rather, the absolute value is controlled by Henry's law constant at the gas-particle interface. Literature data shows that the Henry's law constant of OH and O_3 differ by a ratio of ~4×10^3 (3.8×10^{-1} mol·m^{-3}·Pa^{-1} for OH, 1.0×10^{-4} mol·m^{-3}·Pa^{-1} for O_3 and 5×10^{-3} mol·m^{-3}·Pa^{-1} for O_3 in 1-decane) [43-44], matching quite well when the shape of ρ(r) is similar.

d. Contributions from organic radical species

In the following paragraph we present a possible explanation to the long tail as observed in Fig. 8. Once OH reacts at the aerosol interface a series of free radical intermediates of varying reactivity are produced. A simplified representation of the dominant chemical pathways are shown as R1 to R5.

$$RH + OH \rightarrow R + H_2O \quad (R1)$$

$$R + O_2 \rightarrow RO_2 \quad (R2)$$

$$RO_2 + RO_2 \xrightarrow{1-\alpha} R{=}O + ROH + O_2 \quad (R3)$$

$$\xrightarrow{\alpha} RO + RO + O_2 \quad (R4)$$

$$RO + RH \rightarrow ROH + R \quad (R5)$$

Alkyl radicals (R) are first produced via hydrogen abstraction atom from squalane (RH) by OH. R will react primarily with oxygen, with an estimated lifetime on the order of 10^{-7} s for the oxygen content in the flow tube of ~5×10^{18} cm^{-3}, an assumed rate constant of ~1.7×10^{-11} cm^3·s^{-1} (high pressure limit) [45] and the appropriate Henry's law constant [46]. The reaction between an alkyl radical and other squalane molecules is expected to be much slower, using an extrapolated rate constant of 2.4×10^{-24} cm^3·s^{-1} for the reaction of ethyl radicals with n-hexane [47]. Assuming that the alkyl

radical has a molecular size similar to squalane with a self diffusion constant of 3×10^{-7} $cm^2\cdot s^{-1}$ [30], the corresponding reactive-diffusive length is 3.3 nm. This number when convoluted with the OH concentration profile near the surface gives the spatial distribution of alkyl peroxy radical in the squalane matrix, which is shown in Fig. 9.

The alkyl peroxy radicals can react with HO_2 or another alkyl peroxy radical, with a rate coefficient on the order of 10^{-11} to 10^{-13} $cm^3\cdot s^{-1}$ [45]. The spatial distribution of alkyl peroxy and HO_2 radical does not follow the functional form of other radicals (e.g. OH) and O_3 since the dominant sinks for these species are via self and cross reactions with other RO_2. We instead estimate the steady state concentration of both species under our oxidation conditions using a simple box model. The resulting chemical lifetime for RO_2 corresponds to a reaction-diffusion length of 86 to 400 nm in a squalane matrix, which depends upon the RO_2+RO_2 rate constant. The importance of RO_2+HO_2 channel is suppressed due to the volatility of HO_2 which limits its equilibrium concentration in the aerosol phase. The radial profile of RO_2 is shown in Fig. 9. It becomes apparent that the spatial inhomogeneity of radical propagation from the initial OH reaction is lost over the coating thickness of <12 nm and the RO_2 concentration is expected to be nearly the same throughout the squalane shell. We note here that the RO_2 lifetime due to self reactions is approximately 5×10^{-3} to 2×10^{-4} s, shorter than the fast autoxidation reactions (τ~0.1 s) that are activated by oxygenated groups on the neighboring carbon atoms [48].

The RO_2 self reactions proceed via two major product channels. The RO_2+RO_2 reaction can produce an alcohol and a ketone/aldehyde (R3), or two alkoxy radicals (R4), with O_2 as the coproduct from both reactions. R3 terminates the radical chain chemistry whereas R4 propagates further chemistry in the squalene shell through alkoxy radical reactions. The branching ratio to stable products or alkoxy radicals in the gas phase is a function of molecular structure, but is less

constrained in the condensed phase due to a scarcity of data. In the gas phase, alkoxy radicals can react with oxygen (1.3×10^3 s^{-1}, pseudo first order rate using the same [O_2] as in alkyl radical calculation), undergo unimolecular decompositon (rate of ~10^3 s^{-1}, assuming that RO is not activated by a neighboring oxygenated group) or isomerize (rate of $10^3 - 10^4$ s^{-1}, for carbon chains of 4 or longer) [49]. In the condensed phase there is an additonal bimolecular intermolecular hydrogen abstraction channel due to the high concentration of organic molecules around the alkoxy radical as shown in R5. We estimate the pseudo first order rate of alkoxy radicals due to R5 to be 7.4×10^6 s^{-1} using a second order rate constant of 8×10^5 $M^{-1}s^{-1}$ for the solution phase reaction of cyclohexyloxy radical and cyclohexane.[50] For reference the hydrogen abstraction rate coefficient by tert-butoxyl radical in a variety of solvents is of a similar value [51].

From the time constant analysis outlined above, the reaction of alkoxy radical with surrounding organic molecules should be orders of magnitude faster than competing processes in the squalane shell. Thus if formed by the RO_2+RO_2 reaction, these alkoxy radicals can react with mannitol and extend the reactive-diffusive length beyond the 4 nm coating thickness observed Fig. 8. Whether an alkoxy radical reacts with mannitol core or not is determined by its spatial origin, since the RO reactive-diffusive length is 2.0 nm. In other words, alkoxy radicals produced far away from the core-shell interface will react in the shell before reaching the core. The RO spatial distribution shown in Fig. 9 illustrates this as the concentration decreases within 2 nm of the 10 nm boundary of an infinitely reactive medium towards RO. The values of L for each radical discussed here are summarized in Table 4.

We estimate the contribution of alkoxy reactions at various coating thickness by assuming a branching ratio α in R3 and R4. When combined with the OH only (γ/γ_0) curve, we find a branching ratio of $\alpha = 0.5$ best replicates the experimental measurements. The contribution of RO

radical chemistry to the apparent barrier coefficient is shown as the shaded blue region in Fig. 8. The exact shape of the RO curve is controlled by different factors at either end of the coating thickness scale. When the coating is thin, the RO contribution becomes inversely proportional to the OH contribution because while almost all RO produced can reach the core with high efficiency, the total number of OH reactions within the shell is small. At the other extreme when the coating is thick, the shell consumes most of the OH to produce RO but only those in a relatively small volume (a narrow region adjacent to the core-shell interface) can effectively react with the core and the overall contribution is again decreased.

The formation of alkoxy radical from self-reactions among simple alkyl peroxy radicals is known to occur readily in the gas phase, with a significant yields ranging from 30% to 60% for non-tertiary functional groups on carbon chains up to propane [52]. The production of non-tertiary alkoxy radical is in competition with the formation of the corresponding alcohols and ketone/aldehydes. However, yield data for long chain hydrocarbons is not readily available. Similar channels have also been reported for reactions in the presence of pure organic solvents. For example, Lindsay et al. [53] studied the decomposition products of 1-ethyloxyethyl hydroperoxide in the presence of catalyst near ambient temperature and found the assignment of branching ratios for alkoxy radical production difficult to ascertain due to the subsequent formation of common products from non-radical pathways. A well-constrained number was not given and they suggested a branching ratio (α) between 20% to 80%, assuming low and high concurrent yield of alcohol and carbonyl products from the initially formed alkoxy radical pairs. The more recent work of Li et al. [54] measured the product yield from reactions subsequent to the formation of simple alkyl peroxy radical by catalytic decomposition from the corresponding hydroperoxides in n-alkanes. The products observed include alcohols, carbonyls, acids as well as diols (after post-

processing using lithium aluminum hydride). By considering products associated with hydrogen abstractions to be an indication of the presence of alkoxy radicals, the alkoxy yield from peroxy self-reactions can be estimated. Table 2 in Li et al. [54] listed the decomposition products of 2-hydroperoxy hexane in n-octane measured by gas chromatography after chemical reduction. Assuming the appearance of solvent related alcohols (1-octanol and 2-octanol) to be the result of hydrogen abstraction by 2-hexoxyl radical and the presence of hexane-2,5-diol to be from intra-molecular hydrogen shift of the same radical, we take the summation of the above yields to be divided by the yield of hexan-2-ol, presumably accounting for all other channels giving alcohols and carbonyls. This gives us a rough estimate of the alkoxy branching ratio for low and high initial concentrations of hydroperoxy hexane of 22% and 27%, respectively. Other peroxy radicals studied gave similar yields, such as 4-methyl-2-hydroperoxy pentane in n-octane (17%), 2-hydroperoxy heptane in nonane (11.6%) and 1-hydroperoxy octane in decane (11%). Our estimated branching ratio (50%) appears much higher compared to value from Li et al. [54]. However, we note that a substantial temperature difference exist in experimental conditions between our experiments (20°C) and those by Li (125°C). The temperature dependence of alkoxy radical branching ratio remains unclear [52].

Finally, in a recent stochastic model simulation of aerosol oxidation (squalane) Wiegel et al. [55] found that an alkoxy yield (α) of 10% appeared to provide a good prediction of the experimentally measured average properties such as O/C ratio, molecular weight and aerosol volume. What remains unclear from this computational study is the sensitivity of the model predictions to that exact value of α. In summary, alkoxy branching ratio required to replicate our experimental measurements appears more consistent with gas phase systems and perhaps larger than generally believed for condensed phase reactions. Further measurements of the interfacial

chemistry of alkoxy radicals would be needed to further constrain the overall reactive diffusive length in these systems.

IV. Atmospheric Implications

These measurements of reactive-diffusive length of both ozone and OH provide insights into the diffusive behavior of atmospheric oxidants in aerosols. It has been previously assumed that ozone reactions with condensed phase organics may have a significant bulk component whereas OH reactions occur solely on the surface. Our results show the contrary and that both systems should be considered under a similar framework of which the reactive-diffusive length is the crucial parameter.

Here we considered the reactive-diffusive behavior of small oxidants that originate in the gas phase. The resulting decay in concentration from the gas-particle interface is a direct consequence of the coupling of reactivity with diffusivity, and the concentration profile of the oxidant also corresponds directly to the location where particle phase organic material undergoes reaction. Consequently, there exists two diffusion length scales that affect the overall speed at which an organic particle can be oxidized, in the absence of secondary reactions. For aqueous droplets and liquid-like particles undergoing oxidation in the atmosphere, the diffusive (or mixing) length of the organic material is generally much longer than the aerosol particle dimensions so that spatial distribution of species is homogeneous. An exception occurs after a phase transition, which can lead to phase segregation or crystallization and significantly impact matrix mobility. Indeed, it is under these hindered conditions that the diffusive length of the organic material becomes smaller than the particle radius, [56] or similar to the reactive-diffusive length of the oxidants so that the reactivity of organic material becomes a function of its location in the particle.

As a simple example, we examine a case when an immiscible layer is present on an reactive particle similar to our experimental system as shown in Table 5. Evaporative loss due to oxidation is ignored. The oxidative lifetime of the core material is lengthened, due to transmission loss of gas phase oxidants through the layer. Calculations of an ozone system is based on 500 nm core diameter having the same property of squalene, with an uptake coefficient of 2.7×10^{-3}. For simplicity the non-reactive shell has a diffusivity of 1.6×10^{-6} $cm^2\cdot s^{-1}$ and the reactive shell has a reactive-diffusive length of 1 nm. For OH oxidation the core size is 50 nm with an uptake coefficient of 0.53. The non-reactive shell has a diffusivity of 4.8×10^{-6} $cm^2\cdot s^{-1}$ and the value for reactive shell is calculated with a reactive-diffusive length of 1.4 nm. Lifetime estimates on both are under typical oxidant concentrations in the troposphere. One can generalize the calculation easily for the reactive-diffusive system by assuming exponential decay of core reactivity when the coating thickness is thin relative to the overall size of the particle. The relation is shown in Eq. 5, where τ_0 and τ_{ext} are the oxidative lifetime of the uncoated and coated particle, s the coating thickness and L the reactive-diffusive length of the oxidant in the coating material.

$$\tau_{ext} = \tau_0 \cdot e^{\left(\frac{s}{L}\right)} \quad (5)$$

It is apparent that a purely diffusive shell offers a similar shielding effect as the reactive-diffusive case when the coating is thin, around 1~2 nm. However, when the coating is thick (5 nm) the reactive-diffusive material extends the lifetime by up to a factor of 100 for the case of ozone. We note that for the reactive-diffusive case of OH oxidation with a 5 nm coating the extended lifetime approaches that of the physical lifetime of aerosols (e.g. days to weeks) [57] in urban areas. Aerosol coating therefore provides a modulation mechanism of oxidative lifetime in the atmosphere.

Multiple coating mechanisms exist in the atmosphere. These include deliquescence of material at the particle surface induced by a relative humidity (RH) change, condensation of

secondary organic aerosols onto existing core and solidification as a result of reaction, temperature and RH change. As an example, recent studies on VOC emission by automobiles in California [3] suggested SOA yield due to oxidative processing of unburnt diesel or gasoline emission can amount to concentrations of 10 $\mu g \cdot m^{-3}$, capable of providing aerosol coating in the range of 1 to 2 nm on a 500 nm aerosol core at a number density of 10^3 cm^{-3} and more for smaller core sizes. An increase in lifetime by a factor of 2 to 8 is possible depending on the reactivity and diffusivity of the shielding SOA material. Ultimately, the modification of lifetime can have impacts on the interpretation of atmospheric tracer data as well as estimated age of the aerosols from material decay. Estimation of source strength of organic aerosols can also be affected when the main constraint is the observed organic aerosol mass with age calculated from gas phase tracers.

V. Conclusion

We have successfully utilized core-shell particles to measure transport properties of small oxidants through both diffusive and reactive-diffusive barriers. Our data shows that the reactive-diffusive lengths for OH in squalane and ozone in squalene are surprisingly similar, and that the chemical lifetime of ozone in squalene matrix is much shorter than values extrapolated from gas phase data. With the knowledge of reactive-diffusive lengths, shielding effects on immiscible layers on an reactive substrate can be estimated so that corrections may be made for predictions requiring estimations of oxidative lifetimes.

VI. Acknowledgement

This work is supported by the Department of Energy's Office of Science Early Career Research Program and by the Director, Office of Energy Research, Office of Basic Energy Sciences, Chemical Sciences, Geosciences, and Biosciences Division of the U.S. Department of Energy under Contract No. DE-AC02-05CH11231.

Appendix

A. Derivation of oxidant concentration in core-shell system

This section details the solutions used for constructing concentration profiles in order to calculate the dependence of γ on shell thickness using Eq. 3.

The governing equations for the movement of oxidants in the chemical system under consideration are due to Fickian diffusion and chemical reaction, as shown in Eq. A1.

$$\frac{d\rho}{dt} = D\nabla^2\rho - \frac{\rho}{\tau} \tag{A1}$$

With the assumptions as detailed in the main text, we solve for the time-independent solution by equating the RHS of Eq. A1 to zero. For a single component organic sphere, the steady state oxidant concentration profile can be expressed as Eq. A2 in which r is the radial distance, D the diffusion constant, and τ the chemical lifetime of oxidant in the organic matrix.

$$\rho(r) \propto \frac{\sinh\left(\frac{r}{\sqrt{D\tau}}\right)}{r} \tag{A2}$$

The proportionality constant is determined by the boundary condition, which is the steady state concentration of the oxidant at the particle surface. This value can be further determined by the application of Henry's law constant. The steady state solution is obtained under the assumption that the chemical lifetime of OH is independent of the amount of OH consumed by the aerosol matrix.

Eq. 3 can be used to calculate the γ value representative of the specie being integrated in the numberator, given that the function ρ(r) is known (Eq. A2). Since the expression of Eq. A2 only applies to a sphere of uniform chemical and physical property, solution of ρ(r) for the core-shell system needs to be constructed. Consider the schematic in Fig. 5. For the first case both core

and shell are reactive and are separated at radial distance r_1. The general solutions to each individual domain is of the same form, namely a linear combination of $\frac{\sinh\left(\frac{r}{\sqrt{D\tau}}\right)}{r}$ and $\frac{\cosh\left(\frac{r}{\sqrt{D\tau}}\right)}{r}$, but subjected to different boundary conditions. The inner domain $\rho_1(r)$ which contains the origin requires a vanishing flux at r = 0 and only the hyperbolic sine solution remains. We require the solution in the shell region $\rho_2(r)$ to satisfy the following 2 boundary conditions (Eq. A3 and A4) at r_1:

$$\rho_1(r_1) = \rho_2(r_2) \tag{A3}$$

$$D_1 \frac{d\rho_1}{dr}\Big|_{r1} = D_2 \frac{d\rho_2}{dr}\Big|_{r1} \tag{A4}$$

The overall solution ρ(r) of reactive core shell system is therefore a piece-wise solution consisting of ρ_1 valid in domain $0 < r \leq r_1$ and ρ_2 in $r_1 \leq r \leq r_2$. The expression of ρ_2 is shown in Eq. A5, while ρ_1 is the same as Eq. A2.

$$\rho_1(r) = C\frac{sinh\left(\frac{r}{L_1}\right)}{r}$$

$$\rho_2(r) = \left\{ \frac{sinh\left(\frac{r_1}{L_1}\right)}{sinh\left(\frac{r_1}{L_2}\right)} \cdot \frac{sinh\left(\frac{r}{L_2}\right)}{r} + \frac{r_1 L_2 \left[D_1[1] - D_2[2] \frac{sinh\left(\frac{r_1}{L_1}\right)}{sinh\left(\frac{r_1}{L_2}\right)} \right]}{D_2} \cdot \frac{sinh\left(\frac{r-r_1}{L_2}\right)}{r} \right\} \tag{A5}$$

$$\text{where } [1] = \frac{cosh\left(\frac{r_1}{L_1}\right)}{L_1 r_1} - \frac{sinh\left(\frac{r_1}{L_1}\right)}{r_1^2}$$

$$\text{where } [2] = \frac{cosh\left(\frac{r_1}{L_2}\right)}{L_2 r_1} - \frac{sinh\left(\frac{r_1}{L_2}\right)}{r_1^2}$$

Note that for simplicity, we combine factor $\sqrt{D\,\tau}$ into L, an internal length unit in the reactive-diffusive system, with subscript corresponding to the region. We refer to L as the reactive-diffusive length in this paper. The value C is a constant determined by the concentration of ρ at the surface

($r = r_2$). Fig. 4 shows an example solution to ρ(r) (case 1). Note that we require the oxidant concentration to be continuous at the interface r_1 and the oxidant flux (proportional to the first derivative of ρ(r) times diffusion constant) to match. The discontinuity in slope of ρ at the interface is because of the discontinuity in diffusion constant. If the same D value for both phases are used, the first derivative of ρ(r) will also be continuous at $r = r_1$.

For the second case in Fig. 5, a reactive core is underneath a purely diffusive (non-reactive) shell. In this case ρ(r) can be constructed in a similar manner as the previous case, with the exception that ρ_2 is derived from the solution to a purely fickian diffusion system (no local sink). The solution has the form as shown in Eq. A6 where $\rho_2(r_2)$ is the concentration at the surface and F the total oxidant flux transported through the shell.

$$\rho_2(r) = \rho_2(r_2) - \frac{F}{D}\left(\frac{1}{r} - \frac{1}{r_2}\right) \tag{A6}$$

In joining the solutions representing each region, we apply the same boundary condition at $r = r_1$. An example of the resulting solution ρ(r) is plotted in Fig. 5. Note that the 1/r dependence of ρ in the shell region is a direct consequence of the gradient driven flux transporting oxidant to the core without inherent chemical loss.

The γ value for case 2 is represented as Eq. A7. Since the dependence of γ with the thickness of a non-reactive shell primarily depends on the diffusion coefficient D.

$$\gamma = \frac{4}{r_2^2\langle\nu\rangle} \cdot \frac{H}{\frac{\tau}{K} + \frac{1}{D_2}\left(\frac{1}{r_1} - \frac{1}{r_2}\right) + \frac{4H}{r_2^2\langle\nu\rangle}} \tag{A7}$$

$$\text{where } K = r_1^2 L_1 \frac{cosh\left(\frac{r_1}{L_1}\right)}{sinh\left(\frac{r_1}{L_1}\right)} - r_1 L_1^2$$

This can provide independent information relevant to the reactive shell case where D and τ are always coupled as L. We can then extract the chemical lifetime of oxidants in a concentrated

organic medium without the need of significant extrapolation or fast detection methods.

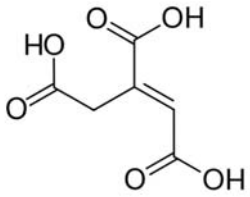

trans-Aconitic acid

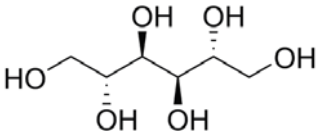

D-Mannitol

Figure 1: Molecular structure of the aerosol core materials.

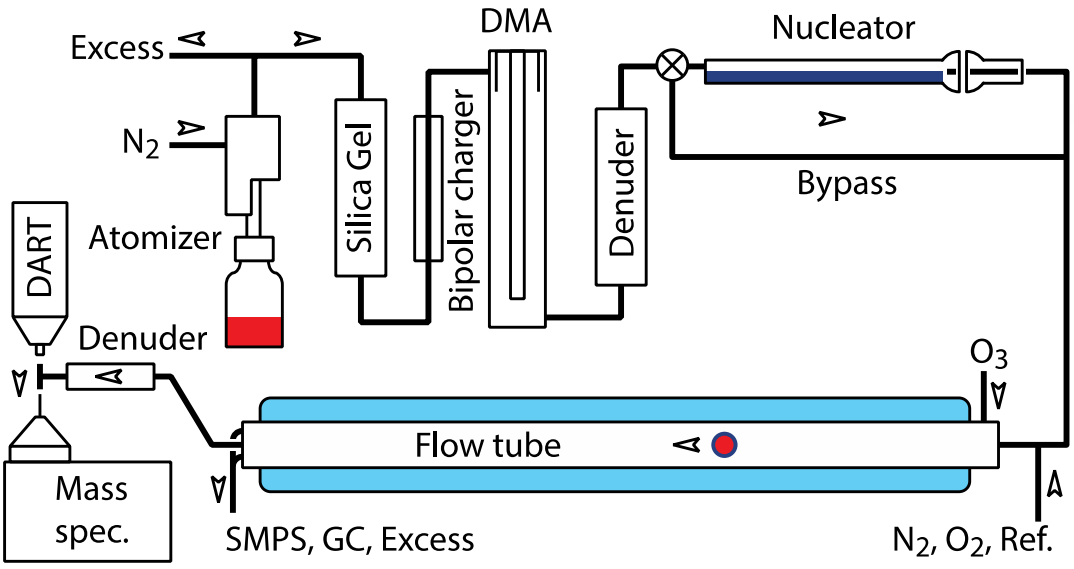

Figure 2

Simplified schematic of instrumental setup. Arrows denote directions of gas flow.

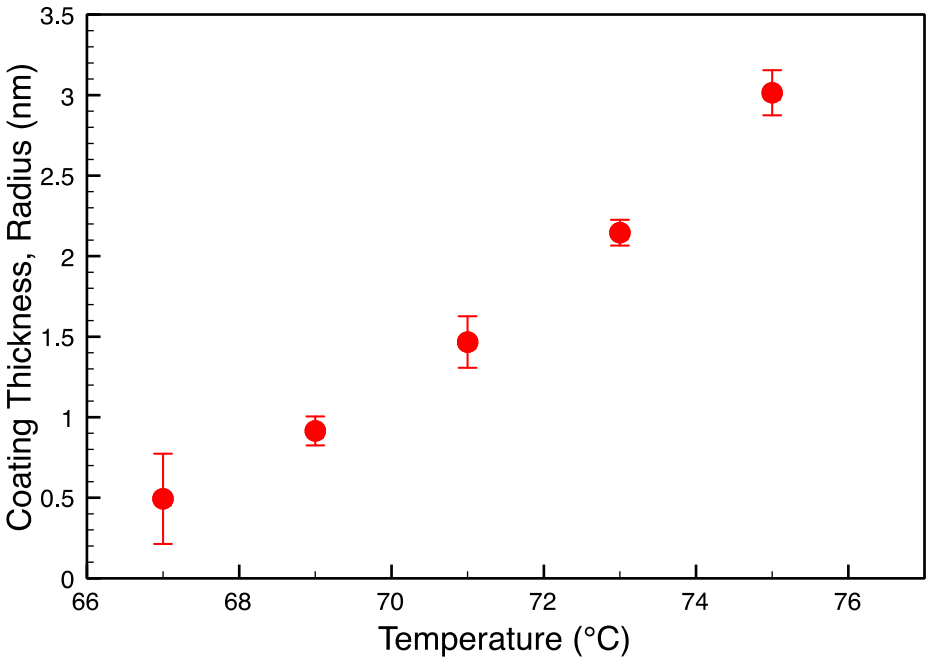

Figure 3

Relationship between nucleator oven temperature and the resulting coating thickness of squalane. The error bar represent the uncertainty at 95% confidence interval.

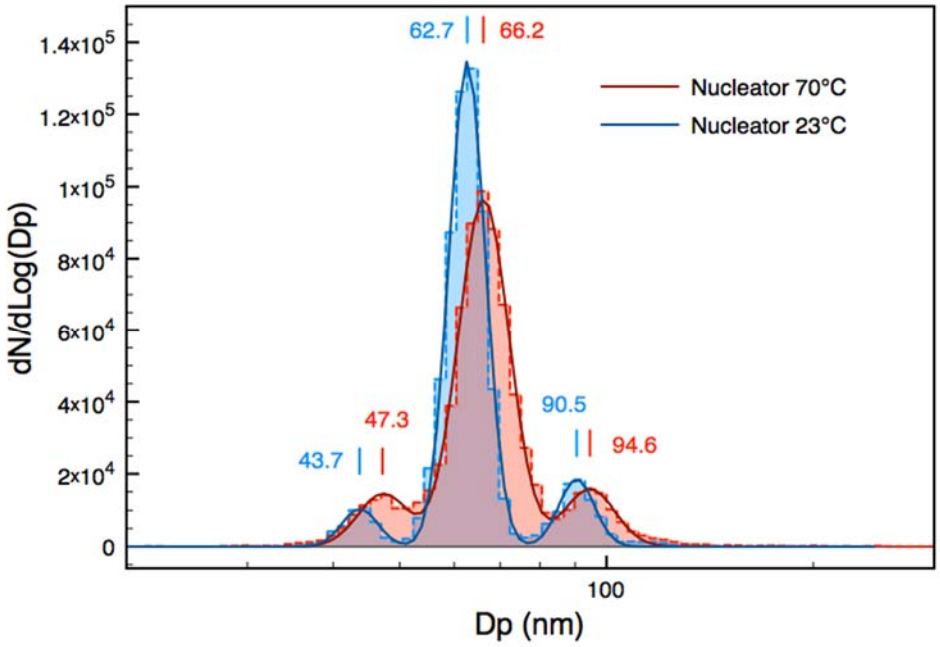

Figure 4

Particle size (in diameter, Dp) distribution of size-selected core before (blue) and after (red) squalane coating using the nucleator oven at the indicated temperature. The particle stream was re-neutralized prior to measurement with a second scanning mobility particle sizer (SMPS) and doubly charged particles through the first and second charging processes are shown as side peaks. Short vertical line marks the center diameter from gaussians fit to data.

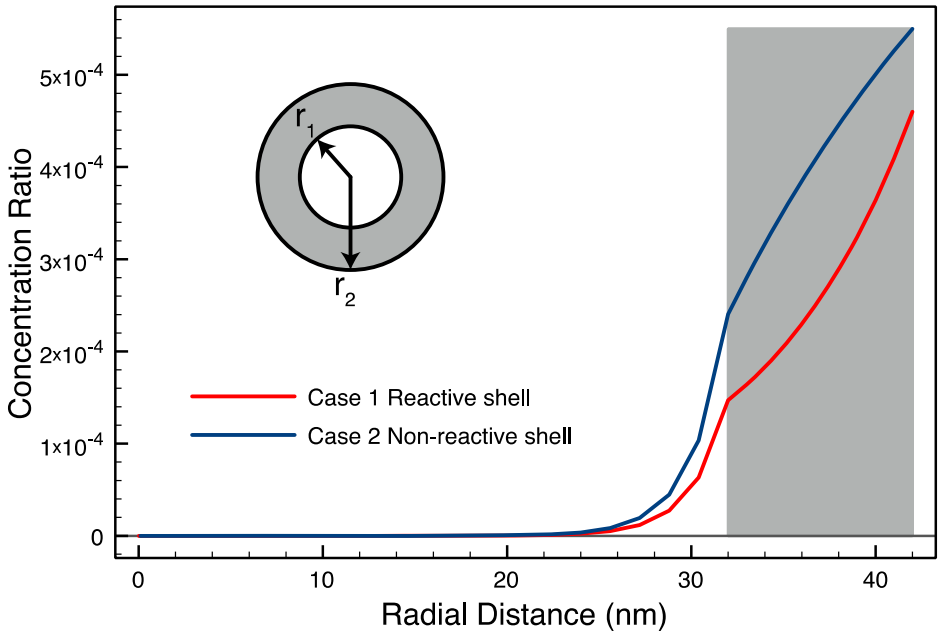

Figure 5

Example solutions of oxidant concentration ρ(r) for the two core shell systems studied in this work. Case 1 represent a reactive core underneath a reactive shell, whereas case 2 represent a reactive core surrounded by a non-reactive shell. The solutions are calculated for a spherically symmetric core-shell particle of 32 nm core radius and 10 nm shell thickness. In this case r_1 = 32 nm, r_2 = 42 nm. The concentration is presented as the ratio in number density of condensed phase to gas phase. The shell region is shaded gray.

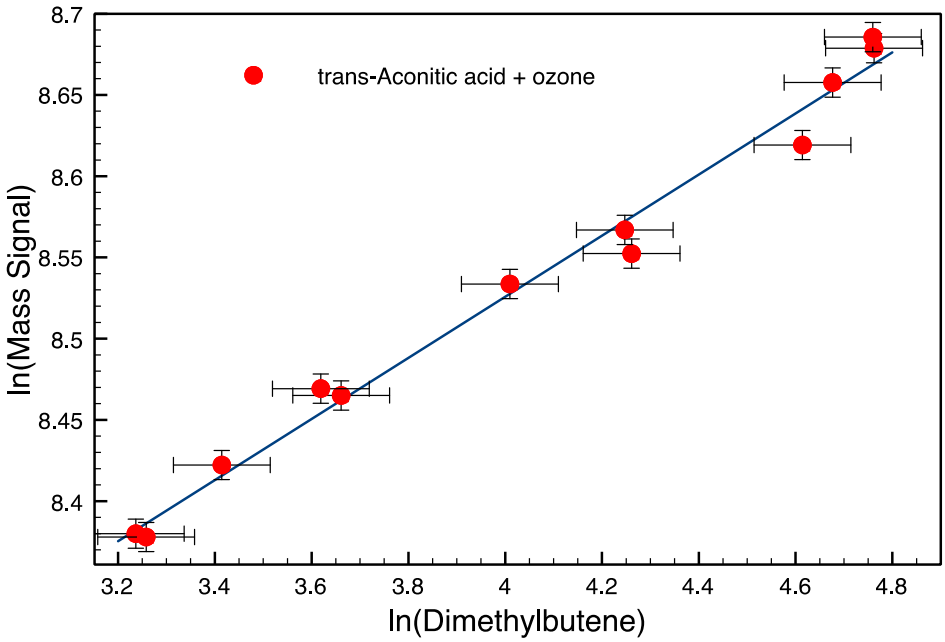

Figure 6

Data from a single point reactive uptake coefficient measurements on *trans*-aconitic acid core of 65.1 nm diameter. *trans*-Aconitic acid was detected by mass spectrometry at m/z=173 in the negative ionization mode.

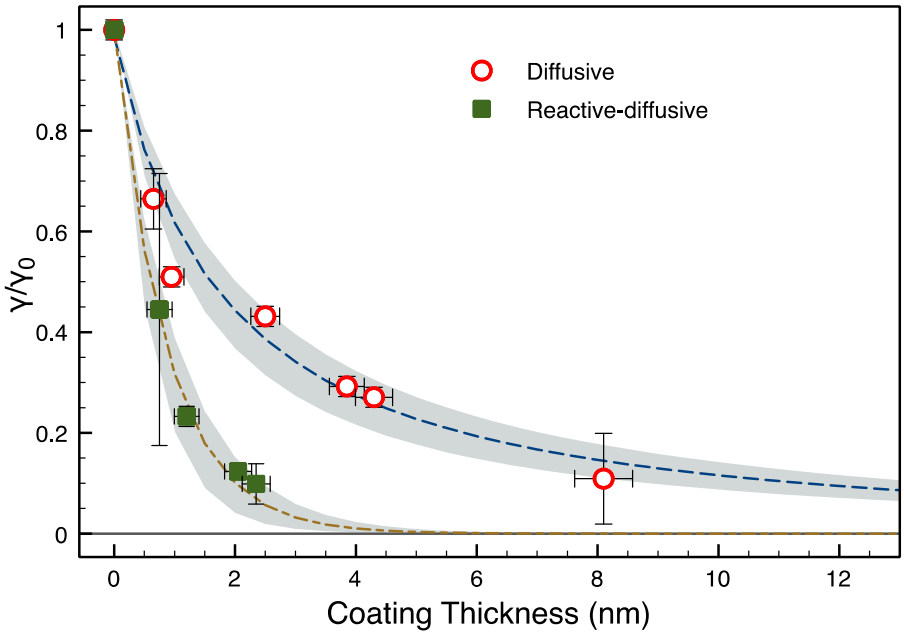

Figure 7

Ozone barrier coefficient (γ/γ_0) through diffusive (squalane, round hollow) and reactive-diffusive (squalene, square filled) organic layers of increasing radial thickness. Best model fit is plotted in dashed lines with shaded areas representing variation of diffusion constant by 30% (diffusive) and reactive-diffusive length by 50% (reactive-diffusive).

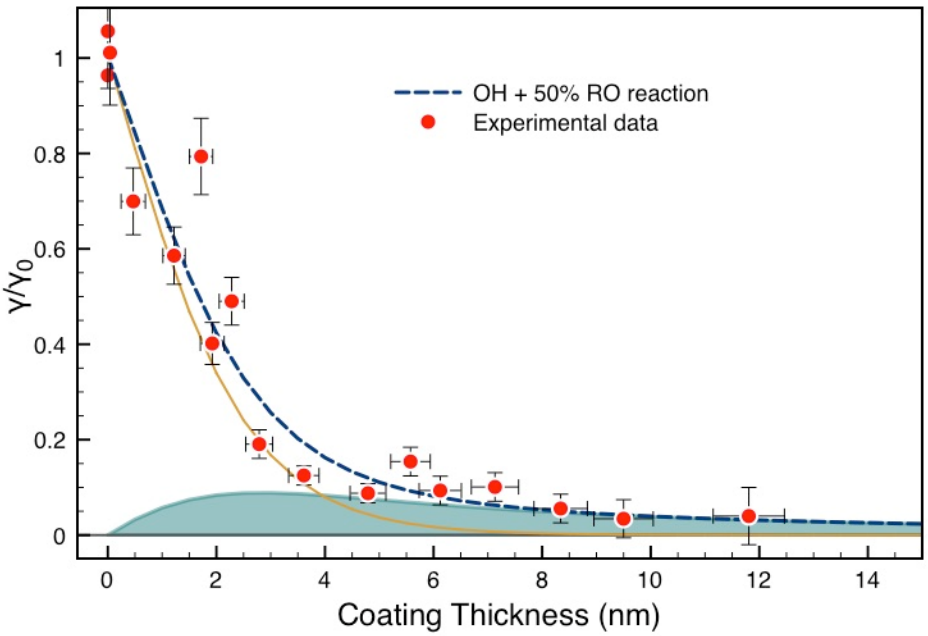

Figrue 8

OH barrier coefficient (γ/γ_0) as a function of squalane coating thickness in radius. The blue dashed trace represents the best fit to the experimental data (round filled) and is constructed as the summation of the golden solid trace (OH contribution) and green shaded area (alkoxy radical contribution) at 50% yield from peroxy radical reactions. See main text for details.

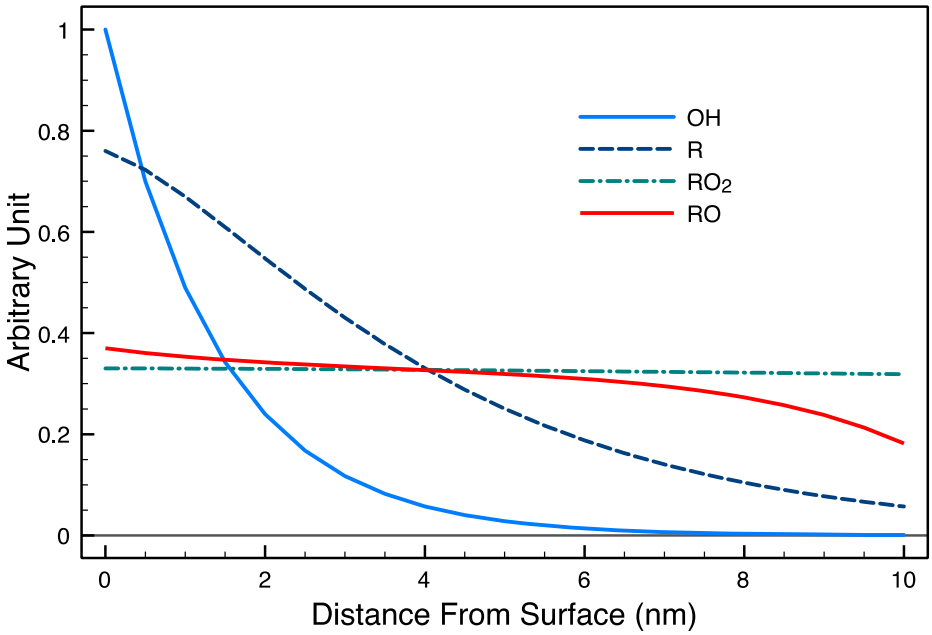

Figure 9

Calculated steady state concentration profiles of OH, alkyl (R), alkylperoxy (RO_2),and alkoxy (RO) radicals in the OH+squalane reaction in an infinite layer 10 nm thick. OH enters the layer from interface at x=0. The reactive diffusive length of various species are taken from Table 4 and the calculated distribution accounts for the spatial spread of the source. For example, the concentration profile of alkyl radical (R) is the convolution of its native decay width due to reactive diffusive length L = 3.3 nm and its source spread (OH) due to OH-initiated hydrogen abstraction reactions.

Table 1. trans-Aconitic acid/squalane + ozone experiments

Exp #	Core diameter nm	Coating[a] nm	Reference compound	$\gamma_{eff} \times 10^{7}$ [b]	$\%(\gamma/\gamma_0)$ (O_3)[c]
1	65.1	0	dmB[d]	5.1±0.1	100%
2	59.9	3.85	dmB	1.5±0.1	29%
3	64.1	8.1	allene	0.56±0.48	11%
4	63.1	2.5	allene	2.2±0.1	43%
5	63.1	4.6	allene	0.52±0.02	10%
6	63.9	4.3	allene	1.4±0.1	27%
7	64.5	0.65	dmB	3.4±0.3	66%
8	64.5	0.95	dmB	2.6±0.1	51%
9	64.8	5.4	dmB	1.5±0.2	29%

a. Coating thickness in radius.
b. Uncertainties are at 95% confidence interval.
c. Calculated by comparing γ to the bare core value in Exp #1.
d. 3,3-dimethyl-1-butene

Table 2. trans-Aconitic acid/squalene + ozone experiments

Exp #	Core diameter nm	Coating[a] nm	Reference compound	$\gamma_{eff} \times 10^{6}$ [b]	$\%(\gamma/\gamma_0)$ (O_3)[c]
1	61.8	0	dmB	1.1±0.1	100%
2	61.8	0.75	dmB	0.48±0.3	45%
3	61.8	1.2	dmB	0.25±0.02	23%
4	61.7	2.1	dmB	0.14±0.01	12%
5	61.7	2.4	dmB	0.11±0.04	10%

a. Coating thickness in radius
b. Uncertainties are at 95% confidence interval.
c. Calculated by comparing γ to the bare core value in Exp 1.

Table 3. Mannitol/squalane + OH

Exp #	Core diameter nm	Coating range[a]		γ
		low	high	
1	104.4	uncoated		0.53±0.04
2	104.4	8.3	11.9	
3	90.0	2.3	4.8	
4	90.0	5.6	7.1	
5	88.5	0	1.9	

a. Coating thickness in radius

Table 4. Reactive-diffusive length of oxidants (radicals) in squalane/squalene inferred from this work

Specie	L (nm)	Dominant sink	Note
O_3	1.0	O_3 + alkene	$D_{O3} = 1.6\times10^{-6}$ cm^2/s
OH	1.4	OH + RH	$D_{OH} = 4.8\times10^{-6}$ cm^2/s
R[a]	3.3	R + O_2	H = 0.22 (O_2 in Toluene)
RO_2[a]	400−86	RO_2 + RO_2	k = 10^{-13} −10^{-11} cm^3/s
RO[a]	2.0	RO + RH	

a. Assuming R is similar in size as squalane.

Table 5. Oxidative lifetime of aerosol under various coating thickness

Oxidant	Coating property[a]	Coating thickness			
		none	1 nm	2 nm	5 nm
$[O_3]$[b] 50 ppb	non-reactive	5 min	11 min	17 min	34 min
	react. L=1 nm		15 min	42 min	12 hr
[OH][c] 10^6 cm^{-3}	non-reactive	33 hr	2.2 day	3 day	6 day
	react. L=1.4nm		2.6 day	5 day	49 day[d]
aerosol conc.	core diameter	equivalent material loading to achieve coating thicknes			
[aerosol] 10^3 cm^{-3}	500 nm		6.3 μg/m^3	13 μg/m^3	32 μg/m^3
	50 nm		65 ng/m^3	136 ng/m^3	380 ng/m^3

a. both reactive and non-reactive coating share the same diffusion constant.
b. calculated for squalene-like aerosol with 500 nm core diameter.
c. calculated for squalane-like aerosol with 50 nm core diameter.
d. approaching the expected lifetime of ambient aerosol.

References

1. Seinfeld, J. H.; Pandis, S. N. *Atmospheric Chemistry and Physics*. John-Wiley & Sons, Inc.: New York, 1998.

2. Bahreini, R.; Middlebrook, A. M.; de Gouw, J. A.; Warneke, C.; Trainer, M.; Brock, C. A.; Stark, H.; Brown, S. S.; Dube, W. P.; Gilman, J. B., et al. Gasoline emissions dominate over diesel in formation of secondary organic aerosol mass. *Geophys. Res. Lett.* **2012,** *39*, L06805.

3. Gentner, D. R.; Isaacman, G.; Worton, D. R.; Chan, A. W. H.; Dallmann, T. R.; Davis, L.; Liu, S.; Day, D. A.; Russell, L. M.; Wilson, K. R., et al. Elucidating secondary organic aerosol from diesel and gasoline vehicles through detailed characterization of organic carbon emissions. *P. Natl. Acad. Sci. USA* **2012,** *109*, 18318-23.

4. Shilling, J. E.; Zaveri, R. A.; Fast, J. D.; Kleinman, L.; Alexander, M. L.; Canagaratna, M. R.; Fortner, E.; Hubbe, J. M.; Jayne, J. T.; Sedlacek, A., et al. Enhanced SOA formation from mixed anthropogenic and biogenic emissions during the CARES campaign. *Atmos. Chem. Phys.* **2013,** *13*, 2091-2113.

5. Worton, D. R.; Isaacman, G.; Gentner, D. R.; Dallmann, T. R.; Chan, A. W. H.; Ruehl, C.; Kirchstetter, T. W.; Wilson, K. R.; Harley, R. A.; Goldstein, A. H. Lubricating oil dominates primary organic aerosol emissions from motor vehicles. *Environ. Sci. Technol.* **2014,** *48*, 3698-706.

6. Worsnop, D. R.; Morris, J. W.; Shi, Q.; Davidovits, P.; Kolb, C. E. A chemical kinetic model for reactive transformations of aerosol particles. *Geophys. Res. Lett.* **2002,** *29*, 57-1-57-4.

7. Moise, T.; Rudich, Y. Reactive uptake of ozone by aerosol-associated unsaturated fatty acids: Kinetics, mechanism, and products. *J. Phys. Chem. A* **2002,** *106*, 6469-6476.

8. Knopf, D. A.; Anthony, L. M.; Bertram, A. K. Reactive uptake of O-3 by multicomponent and multiphase mixtures containing oleic acid. *J. Phys. Chem. A* **2005,** *109*, 5579-5589.

9. Kunzi, L.; Krapf, M.; Daher, N.; Dommen, J.; Jeannet, N.; Schneider, S.; Platt, S.; Slowik, J. G.; Baumlin, N.; Salathe, M., et al. Toxicity of aged gasoline exhaust particles to normal and diseased airway epithelia. *Scientific Reports* **2015,** *5*, 10.

10. Zahardis, J.; Petrucci, G. A. The oleic acid-ozone heterogeneous reaction system: products, kinetics, secondary chemistry, and atmospheric implications of a model system - a review. *Atmos. Chem. Phys.* **2007,** *7*, 1237-1274.

11. Che, D. L.; Smith, J. D.; Leone, S. R.; Ahmed, M.; Wilson, K. R. Quantifying the reactive uptake of OH by organic aerosols in a continuous flow stirred tank reactor. *Phys. Chem. Chem. Phys.* **2009,** *11*, 7885-7895.

12. Waring, C.; King, K. L.; Bagot, P. A. J.; Costen, M. L.; McKendrick, K. G. Collision dynamics and reactive uptake of OH radicals at liquid surfaces of atmospheric interest. *Phys. Chem. Chem. Phys.* **2011,** *13*, 8457-8469.

13. Xiao, S.; Bertram, A. K. Reactive uptake kinetics of NO3 on multicomponent and multiphase organic mixtures containing unsaturated and saturated organics. *Phys. Chem. Chem. Phys.* **2011,** *13*, 6628-6636.

14. Lee, L.; Wooldridge, P.; Nah, T.; Wilson, K.; Cohen, R. Observation of rates and products in the reaction of NO3 with submicron squalane and squalene aerosol. *Phys. Chem. Chem. Phys.* **2013,** *15*, 882-892.

15. Hearn, J. D.; Lovett, A. J.; Smith, G. D. Ozonolysis of oleic acid particles: evidence for a surface reaction and secondary reactions involving Criegee intermediates. *Phys. Chem. Chem. Phys.* **2005,** *7*, 501-511.

16. Najera, J. J.; Percival, C. J.; Horn, A. B. Infrared spectroscopic studies of the heterogeneous reaction of ozone with dry maleic and fumaric acid aerosol particles. *Phys. Chem. Chem. Phys.* **2009,** *11*, 9093-9103.

17. Najera, J. J.; Percival, C. J.; Horn, A. B. Kinetic studies of the heterogeneous oxidation of maleic and fumaric acid aerosols by ozone under conditions of high relative humidity. *Phys. Chem. Chem. Phys.* **2010,** *12*, 11417-11427.

18. Moise, T.; Talukdar, R. K.; Frost, G. J.; Fox, R. W.; Rudich, Y. Reactive uptake of NO3 by liquid and frozen organics. *J. Geophys. Res.-Atmos.* **2002,** *107*, 4014.

19. Zhou, S.; Lee, A. K. Y.; McWhinney, R. D.; Abbatt, J. P. D. Burial effects of organic coatings on the heterogeneous reactivity of particle-borne benzo a pyrene (BaP) toward ozone. *J. Phys. Chem. A* **2012,** *116*, 7050-7056.

20. Zhou, S.; Shiraiwa, M.; McWhinney, R. D.; Poeschl, U.; Abbatt, J. P. D. Kinetic limitations in gas-particle reactions arising from slow diffusion in secondary organic aerosol. *Faraday Discuss.* **2013,** *165*, 391-406.

21. Kolesar, K. R.; Buffaloe, G.; Wilson, K. R.; Cappa, C. D. OH-Initiated heterogeneous oxidation of internally-mixed squalane and secondary organic aerosol. *Environ. Sci. Technol.* **2014,** *48*, 3196-3202.

22. Smith, J. D.; Kroll, J. H.; Cappa, C. D.; Che, D. L.; Liu, C. L.; Ahmed, M.; Leone, S. R.; Worsnop, D. R.; Wilson, K. R. The heterogeneous reaction of hydroxyl radicals with sub-micron squalane particles: a model system for understanding the oxidative aging of ambient aerosols. *Atmos. Chem. Phys.* **2009,** *9*, 3209-3222.

23. Chan, M. N.; Zhang, H.; Goldstein, A. H.; Wilson, K. R. Role of water and phase in the heterogeneous oxidation of solid and aqueous succinic acid aerosol by hydroxyl radicals. *Journal of Physical Chemistry C* **2014,** *118*, 28978-28992.

24. Treuel, L.; Pederzani, S.; Zellner, R. Deliquescence behaviour and crystallisation of ternary ammonium sulfate/dicarboxylic acid/water aerosols. *Phys. Chem. Chem. Phys.* **2009,** *11*, 7976-7984.

25. Leather, K. E.; McGillen, M. R.; Percival, C. J. Temperature-dependent ozonolysis kinetics of selected alkenes in the gas phase: an experimental and structure-activity relationship (SAR) study. *Phys. Chem. Chem. Phys.* **2010,** *12*, 2935-2943.

26. Toby, F. S.; Toby, S. Reaction between ozone and allene in the gas phase. *Int. J. Chem. Kinet.* **1974,** *6*, 417-428.

27. Evans, D. F.; Tominaga, T.; Davis, H. T. Tracer diffusion in polyatomic liquids. *J. Chem. Phys.* **1981,** *74*, 1298-1305.

28. Comunas, M. J. P.; Paredes, X.; Gacino, F. M.; Fernandez, J.; Bazile, J. P.; Boned, C.; Daridon, J. L.; Galliero, G.; Pauly, J.; Harris, K. R., et al. Reference correlation of the viscosity of squalane from 273 to 373 K at 0.1 MPa. *J. Phys. Chem. Ref. Data* **2013,** *42*, 033101.

29. Brabets, R. I.; McDonough, J. M. Density of liquid ozone. *J. Chem. Phys.* **1957,** *27*, 880-882.

30. Kowert, B. A.; Watson, M. B.; Dang, N. C. Diffusion of squalene in n-alkanes and squalane. *J. Phys. Chem. B* **2014,** *118*, 2157-2163.

31. Razumovskii, S. D.; Lisitsyn, D. M. Reactions of ozone with double bonds in polymer and biosystem chemistry. *Polymer Science Series A* **2008,** *50*, 1187-1197.

32. Razumovskii, S. D.; Zaikov, G. E. Influence of structure of unsaturated compound on its reaction rate with ozone. *Zh. Org. Khim.* **1972,** *8*, 464.

33. Epstein, S. A.; Donahue, N. M. The Kinetics of Tetramethylethene Ozonolysis: Decomposition of the Primary Ozonide and Subsequent Product Formation in the Condensed Phase. *J. Phys. Chem. A* **2008,** *112*, 13535-13541.

34. Vereecken, L.; Rickard, A. R.; Newland, M. J.; Bloss, W. J. Theoretical study of the reactions of Criegee intermediates with ozone, alkylhydroperoxides, and carbon monoxide. *Phys. Chem. Chem. Phys.* **2015,** *17*, 23847-23858.

35. Maranzana, A.; Serra, G.; Giordana, A.; Tonachini, G.; Barco, G.; Causa, M. Ozone interaction with polycyclic aromatic hydrocarbons and soot in atmospheric processes: Theoretical density functional study by molecular and periodic methodologies. *J. Phys. Chem. A* **2005,** *109*, 10929-10939.

36. Raff, J. D.; Stevens, P. S.; Hites, R. A. Relative rate and product studies of the OH - Acetone reaction. *J. Phys. Chem. A* **2005,** *109*, 4728-4735.

37. Kessler, S. H.; Smith, J. D.; Che, D. L.; Worsnop, D. R.; Wilson, K. R.; Kroll, J. H. Chemical sinks of organic aerosol: kinetics and products of the heterogeneous oxidation of erythritol and levoglucosan. *Environ. Sci. Technol.* **2010,** *44*, 7005-7010.

38. Airaksinen, S.; Karjalainen, M.; Shevchenko, A.; Westermarck, S.; Leppanen, E.; Rantanen, J.; Yliruusi, J. Role of water in the physical stability of solid dosage formulations. *J. Pharm. Sci.* **2005,** *94*, 2147-2165.

39. Ohmori, S.; Ohno, Y.; Makino, T.; Kashihara, T. Characteristics of erythritol and formulation of a novel coating with erythritol termed thin-layer sugarless coating. *Int. J. Pharm.* **2004,** *278*, 447-457.

40. Easteal, A. J. Tracer diffusion of water in organic liquids. *J. Chem. Eng. Data* **1996,** *41*, 741-744.

41. Rudakov, E. S.; Volkova, L. K.; Tretyakov, V. P. Low selectivity reactions of OH radicals with alkanes in aqueous solutions. *React. Kinet. Catal. Lett.* **1981,** *16*, 333-337.

42. Bartoszek, N.; Ulanski, P.; Rosiak, J. M. Reaction of a low-molecular-weight free radical with a flexible polymer chain: kinetic studies on the OH plus poly(N-vinylpyrrolidone) model. *Int. J. Chem. Kinet.* **2011,** *43*, 474-481.

43. Sander, R. Compilation of Henry's law constants (version 4.0) for water as solvent. *Atmos. Chem. Phys.* **2015,** *15*, 4399-4981.

44. Bin, A. K. Ozone solubility in liquids. *Ozone-Science & Engineering* **2006,** *28*, 67-75.

45. Atkinson, R.; Baulch, D. L.; Cox, R. A.; Crowley, J. N.; Hampson, R. F.; Hynes, R. G.; Jenkin, M. E.; Rossi, M. J.; Troe, J. Evaluated kinetic and photochemical data for atmospheric chemistry: Volume II - gas phase reactions of organic species. *Atmos. Chem. Phys.* **2006,** *6*, 3625-4055.

46. Li, A.; Tang, S.; Tan, P.; Liu, C.; Liang, B. Measurement and prediction of oxygen solubility in toluene at temperatures from 298.45 K to 393.15 K and pressures up to 1.0 MPa. *J. Chem. Eng. Data* **2007,** *52*, 2339-2344.

47. Imbert, F. E.; Marshall, R. M. The mechanism and rate parameters for the pyrolysis of n-hexane in the range 723-823K. *Int. J. Chem. Kinet.* **1987,** *19*, 81-103.

48. Crounse, J. D.; Nielsen, L. B.; Jorgensen, S.; Kjaergaard, H. G.; Wennberg, P. O. Autoxidation of organic compounds in the atmosphere. *Journal of Physical Chemistry Letters* **2013,** *4*, 3513-3520.

49. Atkinson, R. *Gas-Phase Tropospheric Chemistry of Organic-Compounds*. American Chemical Society: 1994; p 216.

50. Druliner, J. D.; Krusic, P. J.; Lehr, G. F.; Tolman, C. A. Generation and chemistry of cyclohexyloxy radicals. *J. Org. Chem.* **1985,** *50*, 5838-5845.

51. Weber, M.; Fischer, H. Absolute rate constants for the beta-scission and hydrogen abstraction reactions of the tert-butoxyl radical and for several radical rearrangements: Evaluating

delayed radical formations by time-resolved electron spin resonance. *J. Am. Chem. Soc.* **1999,** *121*, 7381-7388.

52. Orlando, J. J.; Tyndall, G. S. Laboratory studies of organic peroxy radical chemistry: An overview with emphasis on recent issues of atmospheric significance. *Chem. Soc. Rev.* **2012,** *41*, 8213-8213.

53. Lindsay, D.; Howard, J. A.; Horswill, E. C.; Iton, L.; Ingold, K. U.; Cobbley, T.; Ll, A. Bimolecular self-reactions of secondary peroxy radicals product studies. *Canadian Journal of Chemistry-Revue Canadienne De Chimie* **1973,** *51*, 870-880.

54. Li, J. S.; Pritzkow, W.; Voerckel, V. Intramolecular H-transfer reactions during the decomposition of alkylhydroperoxides in hydrocarbons as the solvents. *Journal Fur Praktische Chemie-Chemiker-Zeitung* **1994,** *336*, 43-52.

55. Wiegel, A. A.; Wilson, K. R.; Hinsberg, W. D.; Houle, F. A. Stochastic methods for aerosol chemistry: a compact molecular description of functionalization and fragmentation in the heterogeneous oxidation of squalane aerosol by OH radicals. *Phys. Chem. Chem. Phys.* **2015,** *17*, 4398-4411.

56. Davies, J. F.; Wilson, K. R. Nanoscale interfacial gradients formed by the reactive uptake of OH radicals onto viscous aerosol surfaces. *Chemical Science* **2015,** *6*, 7020-7027.

57. Gaffney, J. S.; Marley, N. A.; Cunningham, M. M. Natural radionuclides in fine aerosols in the Pittsburgh area. *Atmos. Environ.* **2004,** *38*, 3191-3200.

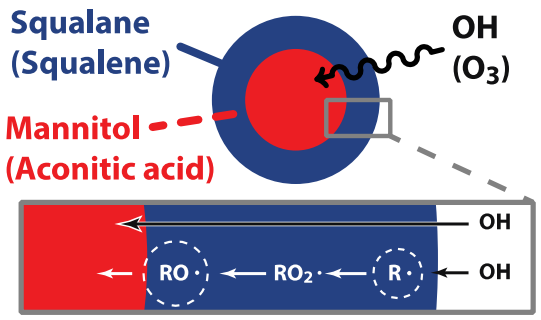
Squalane
(Squalene)
OH
(O_3)
Mannitol
(Aconitic acid)
OH
RO·
RO_2·
R·
OH